Adv. Healthcare Mater. 2017, 1700867

DOI: 10.1002/adhm.201700867

# Heparinization of Beta Tricalcium Phosphate: Osteoimmunomodulatory Effects

*Anna Diez-Escudero, Montserrat Espanol, Mar Bonany, Xi Lu, Cecilia Persson, Maria-Pau Ginebra**

MSc A. Diez-Escudero, MSc M. Bonany, Dr. M.Espanol, Prof. M.P. Ginebra
Biomaterials, Biomechanics and Tissue Engineering Group
Department of Materials Science and Metallurgical Engineering
Universitat Politècnica de Catalunya (UPC), EEBE
Av. Eduard Maristany 10-14, 08019, Barcelona, Spain
E-mail: maria.pau.ginebra@upc.edu

MSc A. Diez-Escudero, MSc M. Bonany, Dr. M. Espanol, Prof. M.P. Ginebra
Barcelona Research Centre for Multiscale Science and Engineering
Universitat Politècnica de Catalunya (UPC), EEBE
Av. Eduard Maristany 10-14, 08019, Barcelona, Spain

Dr. X. Lu, Assoc. Prof. C. Persson
Materials in Medicine Group
Division of Applied Materials Science
Department of Engineering Science, Uppsala University
Lägerhyddsy. 1,751 21, Uppsala, Sweden

Prof. M.P. Ginebra
Institute for Bioengineering of Catalonia (IBEC), Barcelona Institute of Science and Technology
C/ Baldiri Reixac 10-12, 08028 Barcelona, Spain

Keywords: calcium phosphates, heparinization, inflammation, osteogenesis

## Abstract

Immune cells play a vital role in regulating bone dynamics. This has boosted the interest in developing biomaterials that can modulate both the immune and skeletal systems. In this study, calcium phosphates discs (i.e. β-TCP) were functionalized with heparin to investigate the effects on immune and stem cell responses. The results showed that the functionalized surfaces down-regulated the release of hydrogen peroxide and pro-inflammatory cytokines (TNF-α and IL-1β) from human monocytes and neutrophils, compared to non-functionalized discs. The macrophages showed both elongated and round shapes on the two ceramic substrates, but the morphology of cells on heparinized β-TCP tended towards a higher

elongation after 72h. The heparinized substrates supported rat mesenchymal stem cell (rMSC) adhesion and proliferation, and anticipated the differentiation towards the osteoblastic lineage as compared to β-TCP and control. The coupling between the inflammatory response and osteogenesis was assessed by culturing MSCs with the macrophage supernatants. The down-regulation of inflammation in contact with the heparinized substrates induced higher expression of bone related markers by MSCs.

## 1. Introduction

The implantation of synthetic bone grafts in the host bone triggers a complex cascade of events, which ideally should lead either to its osseointegration and/or to its progressive resorption and replacement by new bone. The interaction of the biomaterial with the different cells involved in these events is of paramount importance. However, the attention that has been paid to the different stages of this process has been uneven. Whereas most engineering approaches focus on the osteogenic potential of the material, other crucial events such as their immune response have been often overlooked. The vital role of immune cells in regulating bone dynamics has been emphasized in recent years by the emerging field of osteoimmunology, which has identified the relevant role of immune cells during osteogenesis.[1,2]

After implantation, biomaterials cause a foreign body reaction that can critically determine the success or failure of the material. Briefly, the immune cascade starts with the formation of a transient protein layer on the surface of the biomaterial, followed by extravasation of cells such as neutrophils, monocytes or mast cells that try to phagocytize the biomaterial. At this stage, neutrophils and monocytes release proteolytic enzymes and reactive oxygen species (ROS) such as hydrogen peroxide ($H_2O_2$) to degrade the implant. ROS can cause cell dysfunction and tissue injury depending on the concentration.[3] High concentrations of ROS are deleterious to cells hence an optimal concentration is required to properly modulate the

inflammation cascade by stimulating the balance between pro and anti-inflammatory cytokines. Within a few days, neutrophils undergo apoptosis while monocytes, which have adhered to the substrate, turn into macrophages, which may develop distinct dynamic phenotypes, coded as M1 or M2, with pro-inflammatory or anti-inflammatory functions respectively.[4–7] Whereas the first release chemokines and cytokines that enhance inflammation, the second secrete anti-inflammatory cytokines, and promote bone remodeling and repair, by stimulating osteogenesis and osteoclastogenesis.[8] The polarization of macrophages can be influenced by materials properties. In fact, features such as topography,[9–12] surface chemistry,[13–18] mechanical stimuli,[19,20] or porosity[21,22] are known to drive immune cell fate.

Glycosaminoglycans (GAGs) are interesting as modulator molecules for both immune and skeletal systems. GAGs are ubiquitous in tissues (e.g., as part of stem cells niche and the extracellular matrix, ECM) and are known for their potential to interact with growth factors.[23–25] GAGs assembled into proteins (proteoglycans, PG) are highly present within injured sites. After injury, GAGs are released from their PG back-bone becoming soluble and initiate the healing cascade.[26,27] GAGs can bind chemo- and cytokines that alter leukocyte migration, endothelial extravasation or cytokine expression.[26,28–31] Decades ago, the anti-inflammatory effect of the most sulfonated GAG, heparin, was demonstrated by Dandona *et al*., showing an inhibitory effect on ROS release by leucocytes.[32] In more recent studies, Zhou *et al.* also found a down-regulation of inflammatory cytokines such as IL-1β in presence of GAG multilayers.[33]

Due to their ubiquitous nature, GAGs not only interact with the immune system, but also with bone cells.[34] Their ability to bind proteins and particularly growth factors has been used by several researchers to regulate cell behavior. The degree and position of sulfate groups on GAGs has been shown to influence the affinity for BMPs,[35,36] and to foster osteoblast differentiation[37], by blocking sclerostin which is an inhibitor of Wnt signaling for osteoblast

differentiation.[38] In a similar manner, GAGs can foster osteoclastogenesis blocking osteoprotegerin (OPG), which competes with RANKL, necessary for osteoclast maturation.[39–41]

Overall, the studies performed using GAGs have mostly focused on their supplementation into cell cultures, and little has been done using them as substrates or as surface platforms in combination with biocompatible substrates, besides their application as artificial ECM in combination with collagen or other organic molecules.[24,25,42–46] We hypothesize that the combination of bioactive, osteoconductive and inductive substrates such as calcium phosphate (CaP) materials with the regenerative potential of GAGs can result in an enhancement of their biological performance.

Beta-tricalcium phosphate (β-TCP) as a member of the CaP family is similar to natural bone's mineral phase and has proven success in the clinic for decades. Nevertheless, the main focus of many investigations has been their osteogenic potential, while their interaction with the immune system has often been overlooked. Chen *et al.* have recently made a step forward towards unraveling the tight link between osteogenesis and immunology on ceramic substrates,[17,47,48] mainly β-TCP or porous alumina. However, the studies performed were limited to the evaluation of the effect of β-TCP extracts rather than involving direct cell seeding on the material. The importance of osteoimmunology in the design of bone grafts, and the involvement of GAGs both in inflammatory and osteogenic processes, has encouraged the present work. Some studies have previously explored the functionalization of CaP with heparin, however their focus was on the controlled delivery of pre-load growth factors instead of their recruitment.[42, 51, 52] The aim of this study is devoted to the investigation of the functionalization of β-TCP with heparin as a strategy to simultaneously modulate the response of inflammatory cells (i.e. human neutrophils, monocytes and macrophages), and rat mesenchymal stem cells (rMSC).

## 2. Results

### 2.1. Material characterization

The X-ray diffraction (XRD) analysis revealed that the ceramic discs consisted of phase-pure β-TCP, with all peaks matching those in the JCPDS 09-0169 card (**Figure 1a**). The samples were porous as evidenced by mercury intrusion porosimetry (MIP), with interconnected pores below 1μm (**Figure 1b**). The specific surface area (SSA) of the β-TCP discs was low and typical of high temperature sintered ceramics (**Figure 1c**). The microstructure observed by scanning electron microscopy (SEM) showed the porous nature of the discs and was consistent with the low SSA values from the polyhedral grain microstructure after the sintering process (**Figure 1d**).

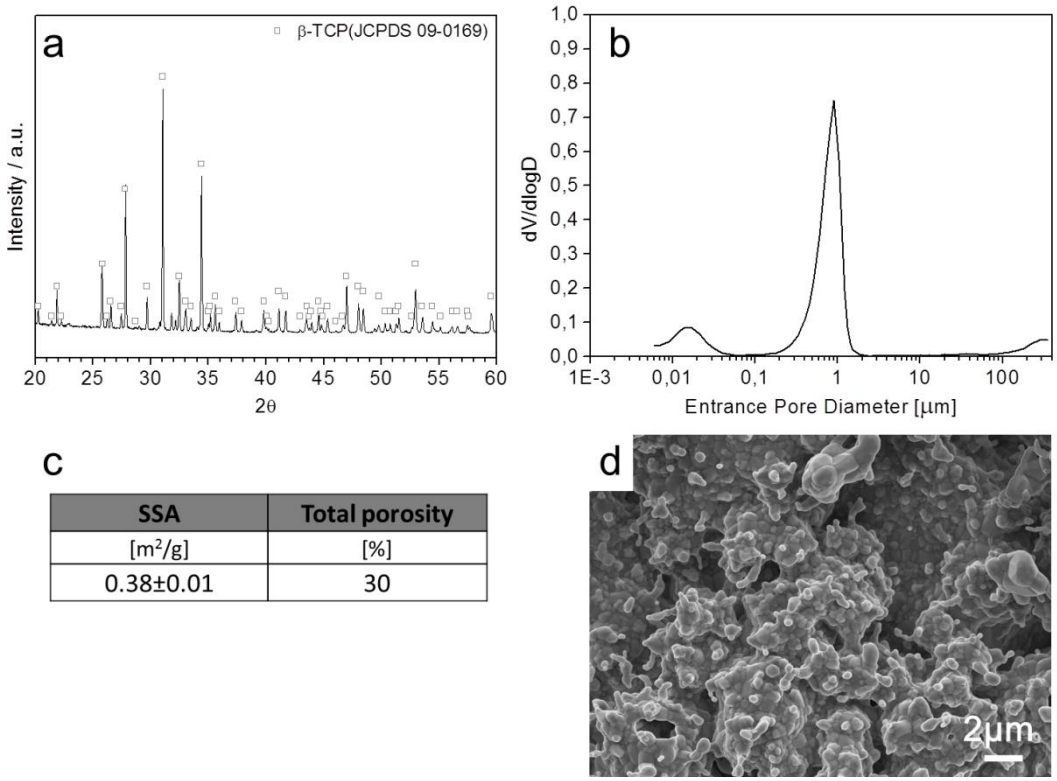


| SSA | Total porosity |
|---|---|
| [m²/g] | [%] |
| 0.38±0.01 | 30 |

**Figure 1.** Physico chemical properties of the β-TCP discs. a) X-ray diffraction pattern; b) Pore entrance size distribution measured by MIP; c) SSA measured by nitrogen adsorption, and total open porosity according to MIP; and d) SEM image of the surface of the material.

### 2.2. Heparin immobilization

The effect of the immobilization method on the amount of heparin retained on the surface is depicted in (**Figure 2a**). The percentage of immobilized heparin (100μg·ml$^{-1}$, 1ml) after 2h

increased drastically when the surface was previously silanized, compared to physical adsorption (**Figure 2a**). Moreover, the silanization time allowed tuning the final amount of immobilized heparin. One hour of silanization followed by two hours of immersion in heparin solution resulted in approximately 10% of the heparin in solution becoming immobilized on the surface. Overnight silanization boosted this percentage up to 30%. Heparin surface saturation studies were performed to investigate the maximum amount of heparin bound to the substrate in two hours, after overnight silanization (**Figure 2b**). As the concentration of heparin in solution increased, the surface reached a saturation value of ~25µg of adsorbed heparin for concentrations of 50µg/ml and above. From X-ray photoelectron spectroscopy (XPS) results, the composition of the substrates displayed mainly calcium, phosphorous and oxygen, which is in agreement with the chemical composition of pristine β-TCP (**Figure 2c**). The detected carbon was attributed to ambient hydrocarbon contamination. The presence of silicon and nitrogen, together with the decrease in Ca and P in the overnight silanized sample (β-TCP-Sil) proved the success of silanization. The increase in carbon content on the silanized substrate was associated to the ethoxy groups present in APTES. The presence of heparin on the heparinized samples (β-TCP-H) was evidenced by the presence of sulphur. The decrease in the ratio of silicon and calcium was associated to the covering of both the substrate and the silane layer by heparin. The SEM micrograph displayed in **Figure 2d** shows that surface functionalization did not induce any morphological change in the substrate.

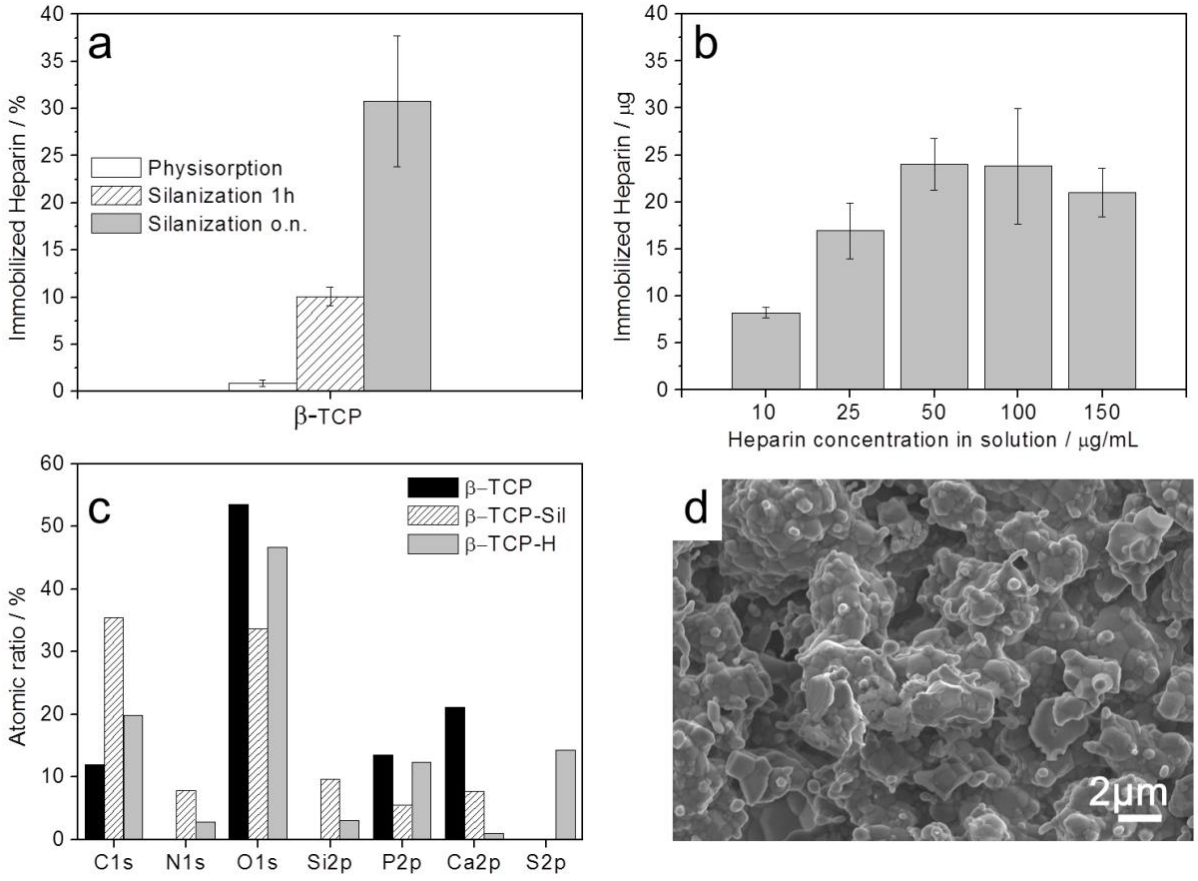


**Figure 2.** Surface functionalization with heparin characterization. a) Effect of the immobilization method on the amount of heparin immobilized on the surface after 2h. The solution used had a heparin concentration of 100µg·ml$^{-1}$. Pristine samples, where heparin was adsorbed by physisorption, are compared to silanized samples, with two different silanization times, 1h or overnight (o.n.); data presented as mean±SD (n=3); b) Saturation of heparin onto the β-TCP surface. The silanized discs (overnight silanization) were immersed for 2h in solutions with different concentrations of heparin; data presented as mean±SD (n=3); c) XPS spectra of the pristine material (β-TCP), overnight silanized β-TCP (β-TCP-Sil) and heparinized β-TCP (β-TCP-H), this last prepared by 2h immersion of o.n. silanized samples in a 150µg·ml$^{-1}$ heparin solution; d) SEM morphology of the surface of β-TCP-H, after heparin functionalization.

**Taking into account the results described above, the heparinization protocol selected for the subsequent cell culture studies consisted in overnight silanization followed by 2h immersion in a 150µg·ml$^{-1}$ heparin solution.**

## 2.3. Cell culture studies

### *2.3.1. Reactive oxygen species generated by monocytes and neutrophils in vitro*

The results of ROS (specifically hydrogen peroxide) release kinetics and total ROS released by monocytes and neutrophils obtained from blood from two donors, following cell activation with phorbol-12-myristate-13-acetate (PMA) are depicted in **Figure 3**. The data for the two

cell types was normalized to the maximum value reached by the positive control, tissue culture polystyrene (TCPS+) and expressed as percentage. Neutrophils showed a delayed release compared to monocytes. β-TCP–H down-regulated inflammation 15% for monocytes and 20% for neutrophils compared to TCPS+. Moreover, the total amount of ROS released by both types of cells when cultured on the heparinized surface, measured as the area below the curve, was lower than when cultured on bare β-TCP or on TCPS+ (**Figure 3b**).

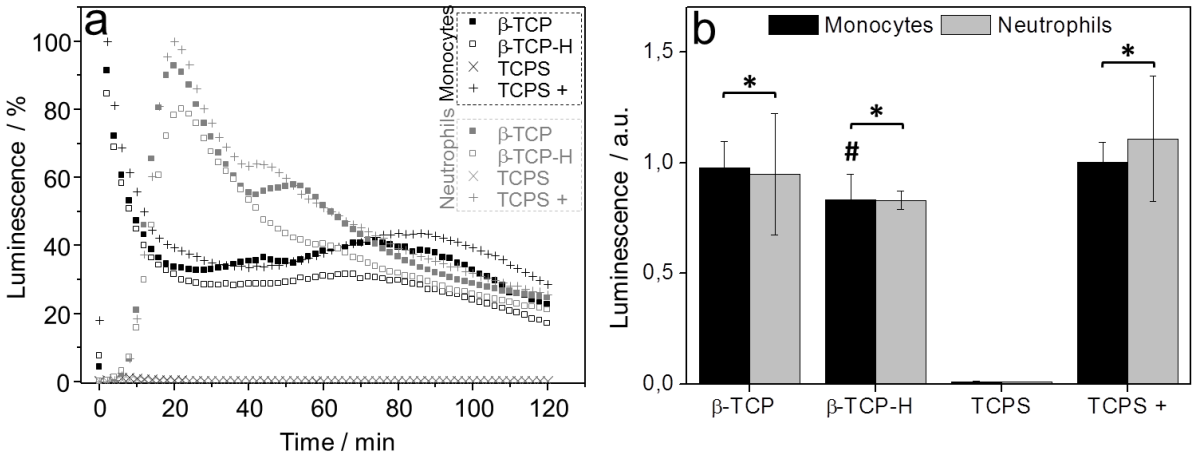


**Figure 3.** ROS release study on PMA-activated cells. Non-activated cells were used as negative control (TCPS). a) $H_2O_2$ release evolution profiles over time; b) Integration of the total area under the curves. Data presented as mean±SD, n=6, *p*-values calculated using one-way ANOVA and Scheffe's post-hoc test, $p < 0.05$. * indicates statistically significant differences compared to the negative control TCPS and # indicates statistically significant differences with respect to β-TCP.

*2.3.2. Macrophage cell culture assays*

Monocytes were seeded on the different substrates, where they adhered turning into macrophages. The release of pro-inflammatory cytokines by macrophages, specifically TNF-α, IL-1β and IL-10, normalized to cell number at each time point, and expressed as fold change with respect to TCPS+/6h (relative fold change) is represented in **Figure 4**. The results were compared to controls with/without lipopolysaccharide (LPS) stimulation (TCPS+ and TCPS, respectively). The cytokine release profile from macrophages for TNF-α and IL-1β confirmed a lower inflammatory response with β-TCP and heparinized β-TCP-H as compared to the positive control TCPS+. β-TCP-H led to statistically significant lower TNF-α level compared

to pristine β-TCP. Moreover, the amount of TNF-α released by macrophages cultured on β-TCP-H was lower than that of the negative control (TCPS). Similar results were observed for IL-1β secretion, which was lowered upon contact with heparinized surfaces, showing slightly lower values than those of control without stimulation (TCPS). IL-10 was not detectable for any of the groups.

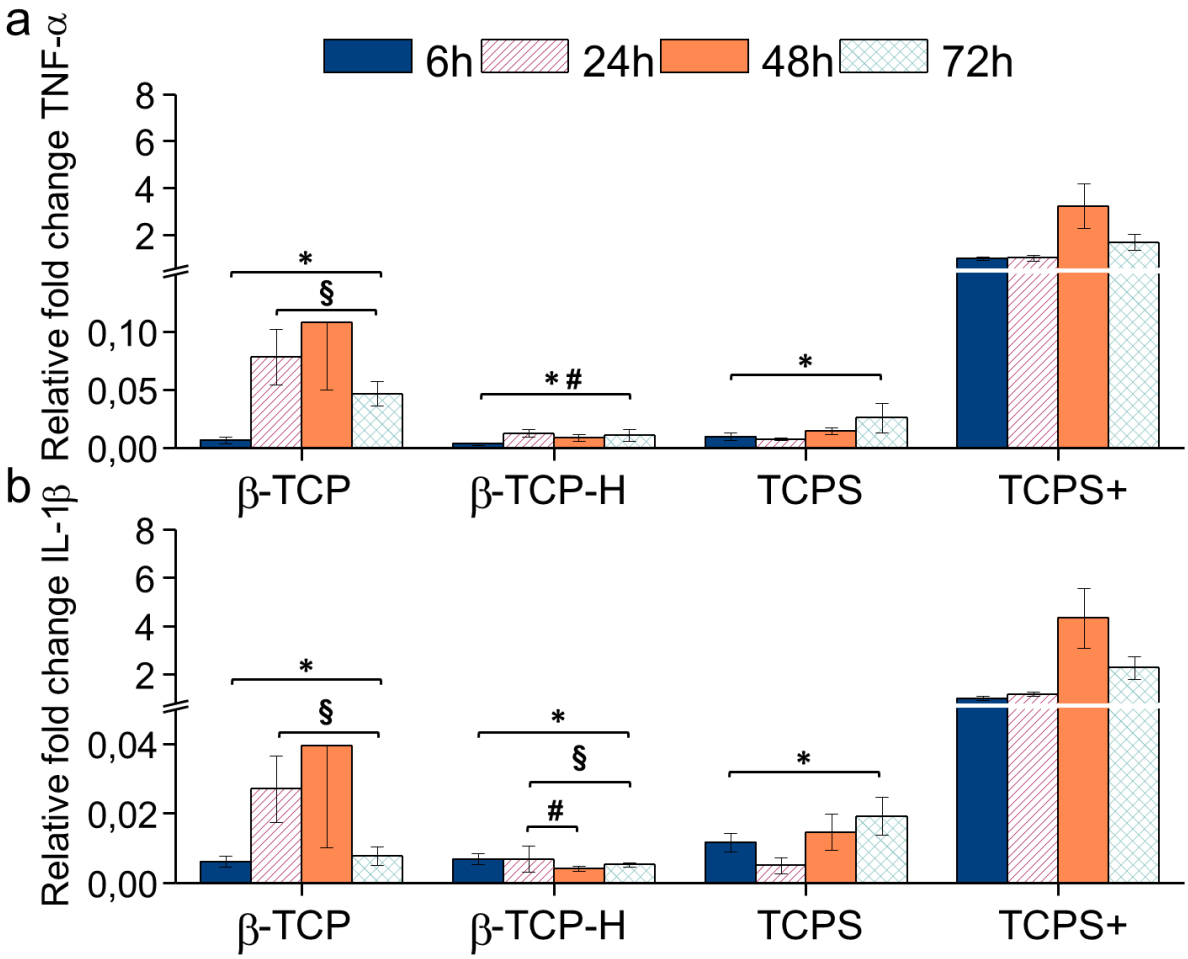


**Figure 4.** Cytokine release by macrophages cultured on substrates for 6, 24, 48 and 72 hours. a) Tumor necrosis factor alpha (TNF-α); b) Interleukin 1 beta (IL-1β). TCPS+ and TCPS correspond to the positive and negative controls, with/without LPS stimulation respectively. * indicates statistical difference compared to positive control TCPS+, § to TCPS and # to β-TCP for each time point ($p<0.05$). Data are presented as mean±SE of duplicate samples from three independent donors (n=6). *p*-values are calculated by one-way ANOVA with Tamhane's post-hoc test.

Macrophage morphology on the different substrates was evaluated by SEM at each time point (**Figure 5**). All substrates promoted macrophage adhesion over time. Some of the cells retained the original round shape whereas others had a more elongated shape. This is relevant

since macrophage morphology can be used to assess phenotype polarization.[52] Cell elongation was observed on both β-TCP and β-TCP-H, whereas TCPS and TCPS+ were prone to form cell clusters. TCPS at 72h (**Figure 5g**) showed flattened cell with no filopodia (**Figure 5g, inset**) which suggest apoptosis, whilst TCPS+ exhibited cells clusters with connecting filopodia (**Figure 5h, inset**). Higher cell elongation was found on β-TCP-H compared to bare β-TCP, which at 72h showed still rounded cells (**Figure 5e** and **f,** red colored). Image analyses of macrophage morphology demonstrated a higher elongation ratio for cells adhered on β-TCP-H (**Figure 5i**), especially at 72h, with a 25% higher elongation rate compared to TCPS.

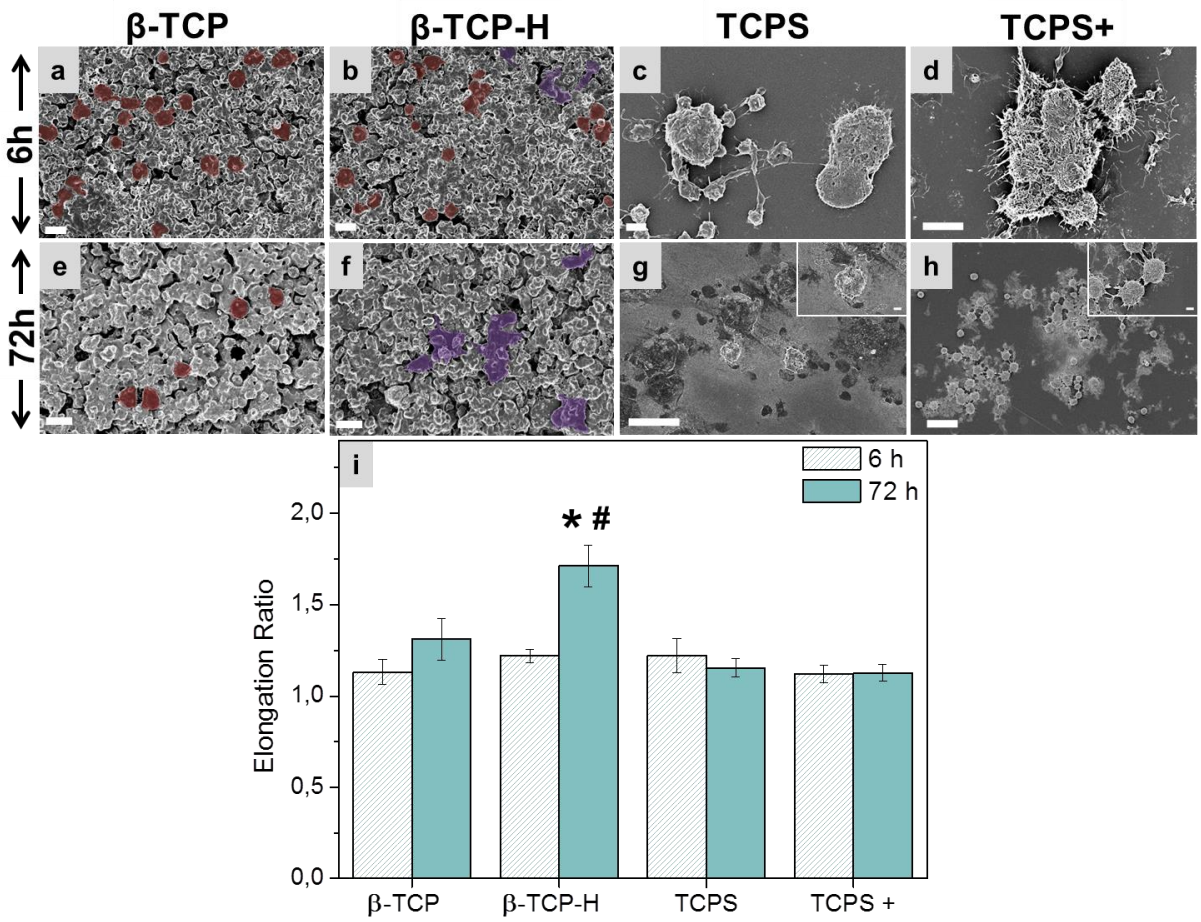


**Figure 5.** Representative SEM images of macrophages on β-TCP at 6h (a) and 72h (e); β-TCP-H at 6h (b) and 72h (f); TCPS at 6h (c) and 72h (g); TCPS+ corresponding to LPS stimulated cells at 6h (d) and 72h (h).Scale bar in images a, b, e, f: 10µm; c, d: 2µm; g, h: 20 µm, inset: 2µm. i) elongation ratio of cells at 6 and 72h. Data represented as mean±SE of a minimum of n=10, and *p*-values calculated by one-way ANOVA with Scheffe's post-hoc test.

* denotes statistically significant differences from TCPS and TCPS+ at 72h, and # statistically significant differences between time points, $p<0.05$.

*2.3.3. Mesenchymal stem cell proliferation and differentiation*

Cell culture with rMSCs showed a slow but sustained proliferation on all β-TCP substrates over 14 days measured by lactate dehydrogenase (LDH), (**Figure 6a**). Cell proliferation studies exhibited no statistically significant differences between β-TCP and β-TCP-H. Lower adhesion on heparinized substrates was found at 6h as well as significant lower proliferation at 7 days comparing both calcium phosphate substrates. Nevertheless, no differences were found at 14 days, where cells proliferation rates were similar, irrespective of functionalization. Both substrates promoted lower proliferation than TCPS, which increased over 7 days until a plateau was reached. The measurement of alkaline phosphatase activity (ALP) demonstrated earlier differentiation on the heparinized β-TCP-H (**Figure 6b**). In the absence of exogenous supplementation, β-TCP-H induced higher differentiation than TCPS at 6 hours and 3 days. After the addition of osteogenic medium (day 4), TCPS exhibit the higher differentiation rate (7 days) compared to calcium phosphate substrates, which decreased at 14 days.

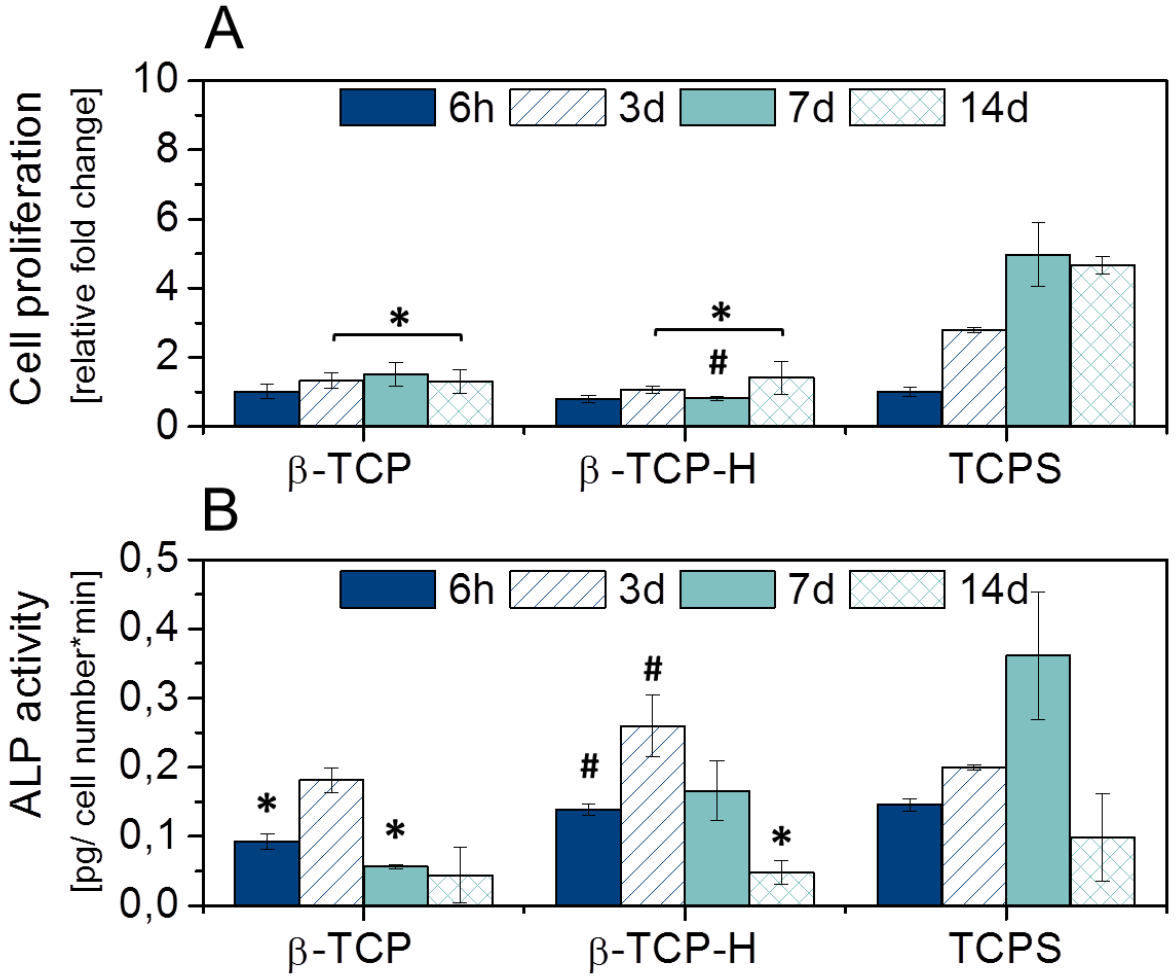


**Figure 6.** Cell proliferation and early differentiation of rMSCs cultured on β-TCP, β-TCP-H and TCPS as control. a) cell proliferation over time (14d) measured by LDH; b) Cell differentiation measured in terms of ALP activity over culture time. On day 4, the cell culture medium was replaced by osteogenic medium. * indicates statistically significant differences compared to control TCPS for the same time point ($p<0.05$) and # indicates statistically significant differences with respect to β-TCP for the same time point ($p<0.05$). Data presented as mean±SD (n=3) and *p*-values calculated by one-way ANOVA with Scheffe's post-hoc test.

*2.3.4. Osteoimmunomodulation of macrophage supernatants on rMSC*

The effect of macrophage supernatants on the gene expression of osteogenic markers by rMSC is depicted in **Figure 7**, including early markers such as alkaline phosphatase (ALP) and collagen type I (COLL) along with late markers such as bone morphogenetic protein 2 (BMP-2) and osteopontin (OPN). β-TCP-H significantly up-regulated the expression of all investigated genes compared to β-TCP at 3 days, although for BMP-2 the results were not statistically significant due to large variation between replicates. TCPS and TCPS+ exhibited

lower expression compared to β-TCP-H after 3 days despite the high values observed at day 1 for BMP-2 and OPN on TCPS+.

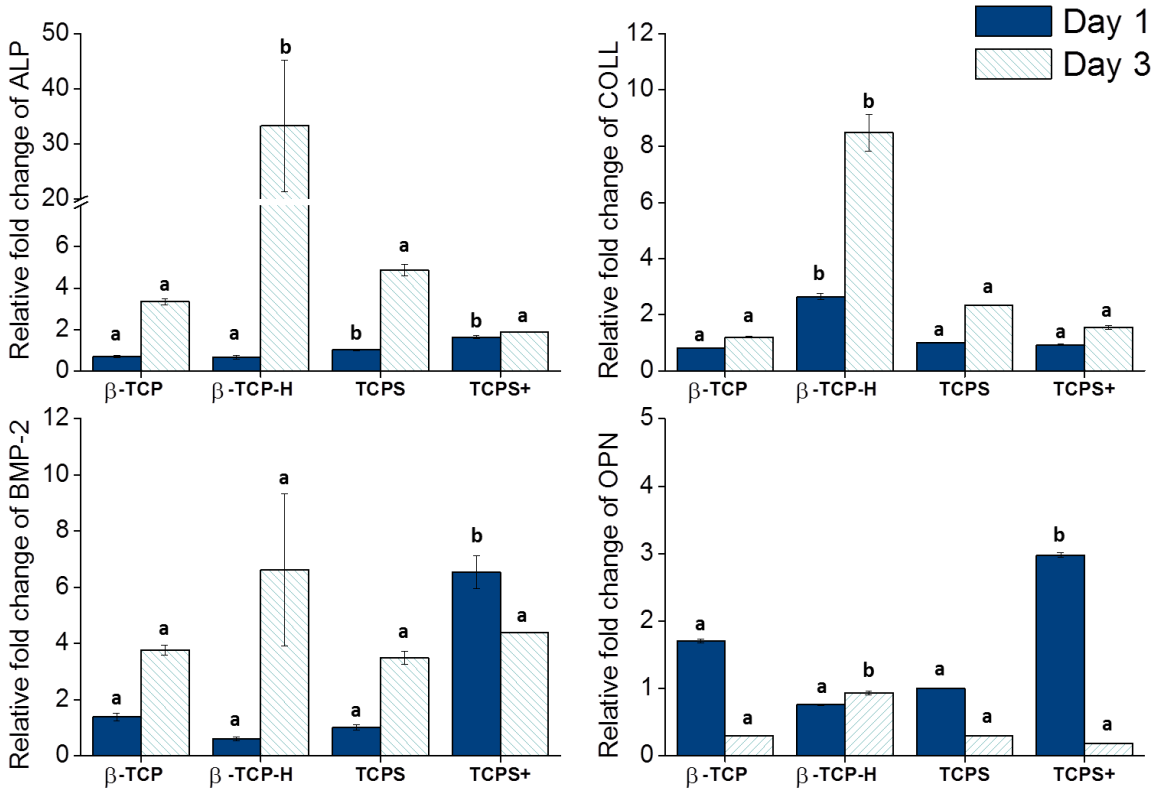


**Figure 7.** Gene expression of rMSC at 1 and 3 days cultured in cytokine containing macrophage supernatants collected at 72h. Letters indicate statistical differences among substrates for each time point ($p<0.05$). Data are presented as mean±SE (n=3) and p-values calculated by one-way ANOVA with Tamhane's post-hoc test.

## 3. Discussion

Calcium phosphates are widely used in clinical procedures. However, although their close resemblance to the composition of bone and other advantages such as bioactivity, osteoconduction and osteoinduction make them good candidates for bone grafting, they are not able to outperform autologous grafts in highly demanding situations. The design of new strategies to foster the interaction with the host tissue during the whole process of bone remodeling may lead to the development of materials with superior performance.

In this context, the present work explores the immune and osteomodulatory effect of heparin immobilized on β-TCP substrates. Heparin is known to have a great affinity to growth factors, and this has been exploited with collagen, polyacrylamide, chitosan and other organic

substrates as a way to stimulate bone regeneration. [25,43,45,53] The high affinity of heparin for growth factors is highly relevant in the case of β-TCP because, even though numerous proteins have high binding affinity to calcium phosphates via amino acids with phosphate- or carboxylate-terminated side chains, most growth factors lack a specific mineral-binding domain.[44] The functionalization with heparin can help to circumvent this limitation. However, studies pertaining to the heparinization of calcium phosphates are scarce, and limited to its use as an anchoring molecule for the immobilization of growth factors on the surface of the biomaterial, for its subsequent delivery.[44,50]

Heparin can bind to CaP by physical adsorption or by covalent attachment, as demonstrated in other works with HA.[50] Physical adsorption of heparin takes place through electrostatic interaction between the charged sulfate/carboxylate groups in heparin with exposed Ca ions on the crystal surface of the CaP. Covalent binding is typically accomplished through a silanization step to covalently graft amine groups that can react with the carboxylate groups from heparin through amide bond formation.[54] Heparin binding through covalent bonds is more stable than physically adsorbed heparin. It has been reported that in complex environments like body fluids, the presence of other charged molecules can compete for binding, thus displacing electrostatically bound heparin from the surface of the CaP.[55] The results obtained in the present work for β-TCP show that a covalent binding yielded higher amounts of heparin than mere physical adsorption. **Figure 2a** shows increased heparin grafting densities following covalent immobilization than physical adsorption, and this was further improved with increased silanization time. The maximum amount of heparin that was adsorbed on the surface of β-TCP was around 25µg, but this dose could be tuned depending on the concentration of heparin used during binding (**Figure 2b**).

To assess the osteoimmunomodulation ability of heparin on β-TCP, covalent attachment was preferred for stability reasons as well as to test heparin's ability to recruit endogenous GF which can help modulate cell function.[53,56] In the present work, primary human cells were

used to assess the inflammatory response of the materials as they reflect better the *in vivo* scenario upon biomaterial implantation. Lower ROS levels were detected after contact with heparinized β-TCP surfaces compared to the non-heparinized ones (**Figure 3b**). The release kinetics were different for the two cell types; whereas neutrophils exhibited a clear monomodal pattern, monocytes showed an acute release within the first 5min followed by a second raise after 80min. Nevertheless, β-TCP-H (**Figure 3a**, blank squares) still displayed the lowest percentage of release. The role of GAGs on inflammation has been previously studied by local administration.[26,31,57] Campo *et al*. found a down-regulation of ROS and inflammatory cytokines in LPS-induced mouse chondrocytes by several GAGs.[31] The highest inhibitory effect was exerted by chondroitin sulfate and heparan sulfate supplementation. Nevertheless, the effect of GAGs has been mainly studied as a supplement in cell culture. Although in the present work the reduction of ROS is low, probably due to low heparin concentration, the trend observed for the heparinized β-TCP surfaces confirm the anti-oxidative activity of heparin.

Activated macrophages secrete cytokines, which also modulate the inflammatory response depending on the interaction with the biomaterial and the implant environment.[58] Mantovani *et al.* extensively described the cytokine system derived from macrophage polarization [4,5] and highlighted the dynamism of this polarization. Even though for decades M1 pro-inflammatory macrophages were seen as mediators of fibrous encapsulation, nowadays it is widely accepted that both M1 and M2 subtypes promote degradation of implants and healing.[59] In the present work, pro-inflammatory (TNF-α, IL-1β), pro-wound healing (IL-1β) and anti-inflammatory cytokines (IL-10) were investigated using primary human cells, which although entailing a certain degree of variability between donors, mimicking more closely the *in vivo* scenario. The cytokine release profiles (**Figure 4**) showed similar trends to those of ROS release. TCPS+ exhibited the highest levels of cytokine release upon LPS stimulation. Neither β-TCP nor β-TCP-H caused cells to secrete more cytokines than LPS-activated TCPS

(TCPS+). Similarly to previous works with β-TCP particles,[60,61] β-TCP substrates induced higher release of TNF-α and IL-1β than TCPS. Functionalization with heparin of these substrates resulted in a reduction of TNF-α and IL-1β release, which was below the levels of TCPS in all three donors for IL-1β, and in two donors for TNF-α. IL-10, an anti-inflammatory cytokine, was not detected by ELISA in any of the substrates. Overall, the reduction in the inflammatory response caused by heparin on the surface of the β-TCP substrate was in agreement with previous results obtained in GAG multilayer substrates by Zhou *et al*.[33]

Besides the cytokines release profile, cell shape can provide information on macrophage phenotype. Sridharan *et al.* concluded that macrophage elongation can be associated to a pro-healing phenotype (M2), whereas pro-inflammatory macrophages (M1) present more rounded shapes.[62] Similarly, McWorther *et al.* found elongated shapes being compatible with an expression of M2 phenotype on patterned TCPS.[52] SEM images showed early elongation on β-TCP substrates at 6h (**Figure 5a and b**), which continued up to 72h, more pronounced on heparinized β-TCP-H (**Figure 5e and f**). Image analyses of cell morphology revealed significantly higher elongation ratio for β-TCP-H at 72h (**Figure 5i**), which can be related to M2 polarization, in agreement with the lower cytokine release (**Figure 4**).

Osteogenic cell proliferation and differentiation are required to continue the healing process. Some studies performed by supplementing GAGs into the cell media or by attaching them on TCPS have determined that the binding affinity between GAGs and osteogenic markers such as osteocalcin, osteonectin or osterix, is necessary for osteoblast maturation.[63,64] The use of osteoconductive substrates such as CaPs in combination with GAGs can further enhance their biological response. β-TCP and TCPS showed similar rMSCs adhesion, while a slightly lower cell adhesion was found for heparinized β-TCP-H, even though no significant differences were found in the statistical analyses (**Figure 6a**). Noteworthy, early differentiation was stimulated by the presence of heparin as there was increased ALP activity compared to pristine β-TCP, evidencing an early effect on MSC differentiation by the heparinized platform

itself (**Figure 6b**). Although after osteogenic stimulation (7 and 14 days) ALP expression was higher on TCPS this might be influenced by cell confluence, as denoted by the plateau reached in cell proliferation for TCPS (**Figure 6a**). The coupling of inflammation and osteogenesis investigated through the cytokine containing supernatants from macrophage cell cultures evidenced a pro-osteogenic effect on rMSC (**Figure 7**). A higher expression of osteogenic markers (ALP, COLL, BMP-2 and OPN) was observed when MSCs were in contact with the supernatants of macrophages cultured on heparinized β-TCP compared to β-TCP, which can be associated with the lower release of pro-inflammatory cytokines as a consequence of heparinization. These results are in accordance with previous works that found higher expression of bone-related markers by MSCs cultured with the supernatants of inflammatory murine cells in contact with β-TCP.[47] Unexpectedly, high expression of late markers was found for β-TCP and TCPS+ at day 1 even if both substrates showed high levels of pro-inflammatory cytokines, which should be further investigated.

Overall, the results obtained here support the functionalization of CaP with heparin as an osteoimmunomodulatory strategy. Heparinization of CaPs supported MSC adhesion, proliferation and differentiation, together with a down-regulation of oxidative stress and pro-inflammatory cytokines, which in turn, promoted osteogenesis. Whether this synergy between down-regulation of inflammation and pro-osteogenic effect can foster bone healing at different stages of remodeling requires further *in vitro* investigations and rigorous *in vivo* testing.

## 4. Conclusion

Heparin was covalently attached on β-TCP substrates by a silanization process and achieved significantly higher grafting densities compared to physisorption. The presence of heparin clearly influenced the response of both immune and osteogenic cells. Heparinization decreased the levels of hydrogen peroxide and inflammatory cytokines released from human immune cells in contact with the material. Cells elongation ratio was found to be higher on

heparinized β-TCP-H, which denotes a M2 or pro-healing phenotype correlated to the down-regulation of pro-inflammatory cytokines. This down-regulation of inflammation was connected to higher expression of osteogenic markers in MSCs and is compatible with pre-osteoblastic differentiation. In addition, heparinized substrates enhanced mesenchymal stem cell differentiation, as shown by higher ALP expression after 3 days of culture without osteogenic medium.

## 5. Experimental Section

*Preparation of calcium phosphates*: β-TCP was obtained by sintering calcium deficient hydroxyapatite (CDHA). CDHA discs were obtained by hydrolysis of alpha-tricalcium phosphate (α-TCP) through a self-setting reaction. α-TCP was prepared by solid state reaction of calcium hydrogen phosphate ($CaHPO_4$, Sigma-Aldrich, St. Louis, USA) and calcium carbonate ($CaCO_3$, Sigma-Aldrich, St. Louis, USA) mixed at a 2:1 molar ratio and heated for 15h at 1400°C followed by quenching in air. Subsequently, the particles obtained were milled to a final median size of 5.2µm[65] and mixed with 2wt% of precipitated hydroxyapatite (PHA, Merck KGaA, Darmstadt, Germany). This powder was then mixed for 1 minute in a mortar with distilled water at a liquid to powder ratio (L/P) of 0.35 $ml \cdot g^{-1}$, resulting in a paste that was transferred into 15x2 and 5x1 $mm^2$ PTFE moulds. The discs were immersed in water at 37°C for 10 days, to allow for complete hydrolysis to CDHA. The discs were subsequently subjected to a sintering process at 1100°C for 9h to obtain the final β-TCP.

*Heparinization:* Heparin immobilization on the surface of β-TCP was performed using two different routes, either physical adsorption or chemisorption, i.e. chemical covalent binding (**Figure 8a** and **b**, respectively). Freshly prepared heparin (BioIberica S.A.U. Barcelona, Spain) solutions in phosphate buffer saline (PBS, Thermo Fisher Scientific) were used. Physical adsorption was carried out by immersing the samples in the heparin solution or 2 hours under gentle agitation (100 rpm). Heparin covalent binding was accomplished via a 2-

step functionalization method: i) First, silanization with APTES was performed using a modified procedure from previous work.[66] Discs were immersed in a solution of APTES (2% vol., i.e. 80 mM) in absolute Ethanol (Panreac,AppliedChem) in the presence of distilled water (3% vol.) and left for different times (1 hour or overnight) under agitation. Afterwards, the discs were removed and sonicated in an ultrasonic bath (Ultrasons-HD, J.P. Selecta, Barcelona) in absolute ethanol solution for 5min, followed by three ethanol rinses to remove any unbound APTES; ii) The second functionalization step consisted in the covalent immobilization of heparin onto the aminated surfaces of the materials. Carbodiimide (1-(3-dimethylaminoporpyl)-3-ethylcarbodiimide, EDC, Sigma-Aldrich, St. Louis, USA) and *N*-hydrosuccinimide (NHS, Sigma-Aldrich, St. Louis, USA) were used to couple heparin via its carboxyl groups to the amino groups of the silane. Freshly prepared solutions of heparin in PBS at different concentrations were firstly activated for 15min at pH ~6.5 in presence of EDC/NHS (100 and 150 mM, respectively). Upon activation, pH was raised to 7.5 and the silanized discs were immersed in the activated heparin solution (1ml) for 2h under agitation (100rpm).

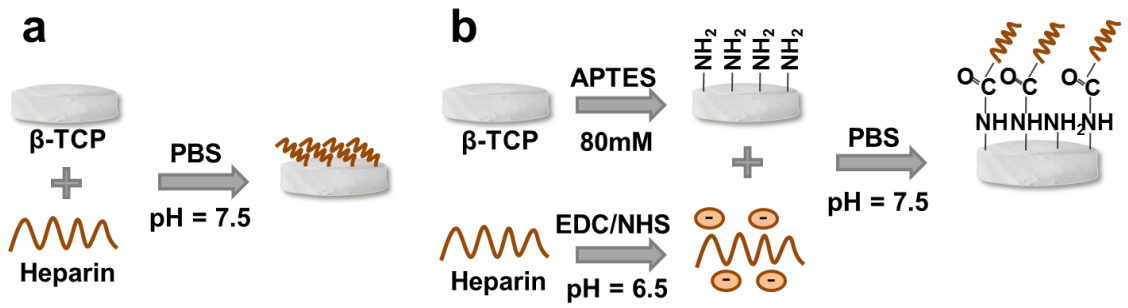


**Figure 8.** Diagram of the two heparin immobilization methods. a) physisorption and b) chemisorption.

The heparin saturation curves were determined on the overnight silanized surfaces by immersing the samples in activated heparin solutions with different concentrations (10, 25, 50, 75, 100, 150, and 200µg·ml$^{-1}$) for 2h. Supernatants were collected, and the amount of heparin was determined using a colorimetric assay modified from the literature.[54] Briefly, a solution

of 0.005wt% Toluidine blue (Sigma-Aldrich, St. Louis, USA) was prepared in 0.01M hydrochloric acid (HCl, PanreacAppliChem) and 0.2wt% sodium chloride (NaCl, Sigma-Aldrich, St. Louis, USA). Heparin supernatants were mixed with the Toluidine solution at a 1:1 ratio, vortexed and centrifuged for 5 min at 15000 relative centrifugal force (rcf). Afterwards, 200 µL of the sample solutions were placed in a 96-wellplate and the absorbance was read at 631nm (Infinite 200 PRO Microplate reader, TECAN). A standard calibration curve was made, measuring solutions with known heparin concentrations up to 25µg·ml$^{-1}$.

*Materials characterization:* The SSA of the discs was measured by nitrogen adsorption using the Brunauer-Emmett-Teller method (ASAP 2020 Micromeritics). The porosity and pore size distribution were obtained by MIP analyses (Autopore IV Micromeritics). Phase composition was assessed by XRD (D8 Advance, Bruker) using a Cu Kα anode operated at 40kV and 40mA. Data were collected in 0.02° steps over the 2θ range of 10°-80° with a counting time of 2 per step. Phase identification was accomplished comparing the resulting patterns to that of β-TCP (JCPDS 09-0169).

SEM (FIB Zeiss Neon40) was used to study the microstructure of the samples, previously coated with carbon to enhance conductivity. The microstructure of the samples was studied before and after functionalization to investigate possible morphological changes. XPS was used to analyze surface composition of the pristine (control) and functionalized samples. Spectra were acquired in ultra-high vacuum ($5\cdot10^{-9}$mbar) with an XR50 Mg anode source operating at 150 W and a Phoibos 150 MCD-9 detector (D8 advance, SPECS Surface Nano Analysis GmbH, Germany). Spectra were recorded at pass energy of 25eV with a step size of 0.1eV for C1s, N1s, O1s, Si2p, Ca2p, P2p, and S2p. C1s peak was used as a reference. CasaXPS software (Casa Software Ldt, UK) was used for the determination of atomic elemental composition applying the manufacturer set of relative sensitivity factors.

*Cell isolation:* The inflammatory response was evaluated using primary human cells isolated from blood obtained from anonymous volunteer donors at the Uppsala University Hospital.

Human monocytes and neutrophils were isolated from buffy coats by two different separation procedures. Firstly, monocytes were isolated from blood (15ml) which were then diluted in 1xPBS at a 1:1 ratio and mixed gently by inversion. Afterwards, diluted blood (30ml) were gently poured onto Ficoll-Paque Plus (15ml) (GE Healthcare, Chicago USA) followed by centrifugation at 400 rcf for 30min. The upper human plasma layer was collected and kept at 4°C for later use. The monocyte layer was collected and resuspended in 1xPBS (10ml) and centrifuged at 100 rcf for 15min for a total of 3 washes. Next, the monocyte pellet was resuspended in PBS (2ml) and the cells were counted by Trypan blue exclusion method (1:5) in a hemocytometer. Finally, cells were diluted in cell culture medium (4PBS/1RPMI-1640/100mM glucose) containing 10% of human plasma.

Secondly, to extract the neutrophils, the blood pellet layer obtained after centrifugation and removal of plasma and the mononuclear layer was resuspended in 20ml of 3% Dextran (Sigma) in 0.9% saline solution and incubated for 25min. The supernatant was collected and centrifuged at 250rcf for 10min. Afterwards, the supernatant was treated with 20ml of 0.2% saline for 20s, followed by 20ml more of 1.6% saline in order to lyse erythrocytes. The cell suspension was then centrifuged at 250 rcf for 10min. The neutrophil pellet was resuspended in PBS and cells were counted using acetic acid (6%) in a cytometer. Finally, cells were diluted in cell culture medium (4PBS/1RPMI-1640/100Mm glucose) with 10% of human plasma.

*Chemiluminescence study:* A luminol amplified chemiluminescence assay was used to quantify the ROS generated by both monocytes and neutrophils[67,68]. Prior to the analyses, the 5x1mm$^2$ discs were sterilized in 70% ethanol for 3h, followed by three PBS rinsings of 15 min each. 200µL of cells were seeded on the pristine and heparinized β-TCP discs at a cellular density of $10^6$cells·ml$^{-1}$, followed by the addition of 100µL of 500µM luminol solution. Previously, a luminol solution was prepared by adding 1% of luminol stock solution and 0.2% horseradish peroxidase (1mg·ml$^{-1}$, Jackson Immuno Research) as signal amplifier. The

luminol stock solution was obtained by dissolving luminol (Fisher Scientific) to 50mM in 0.2M NaOH. Both cell types and positive controls (TCPS+) were activated with 1µM PMA (Sigma Aldrich), which was added into the luminol solution. A negative control consisting of non-activated cells seeded on TCPS. Luminescence was monitored in a microplate reader (Infinite M200, Tekan, Männedorf, Switzerland) at 37ºC every 2 min up to 2h. Measurements were conducted using triplicates and two independent blood donors for each cell type.

*Macrophage cell culture:* Macrophage cell culture assays were performed using 15x2 $mm^2$ discs. Upon isolation, monocytes were resuspended in complete RPMI cell culture medium supplemented with 10% fetal bovine serum (FBS, Thermo Scientific Hyclone), 2% HEPES (Sigma-Aldrich, St. Louis, US) and 1% Penicillin/streptomycin (Thermo Scientific). Prior to seeding, pristine and heparinized β-TCP discs were sterilized as previously described and immersed overnight in 1ml of complete medium. Seeding was performed by adding 1ml of cells in complete medium ($2\cdot10^5$cells$\cdot$$ml^{-1}$). All substrates were supplemented with 1ng$\cdot$$ml^{-1}$ of LPS (Sigma-Aldrich, St. Louis, US) including a positive control (TCPS+). The negative controls (TCPS) consisted in cells without LPS supplementation. Cells were cultured for 3 days. Supernatants of macrophage cultures were collected at 6, 24, 48, and 72h, centrifuged at 1500rpm and analyzed with ELISA kits to detect Tumor Necrosis Factor (human TNF-α, KHC3012, Invitrogen), Interleukin 1 (human IL-1β, KHC0012, Invitrogen) and Interleukin 10 (human IL-10, KHC0103, Invitrogen). Duplicates were used for each single experiment and three biological replicas were conducted with three independent blood buffy coats. The results were normalized to cell number at each corresponding time point.

Cell viability at each time point was quantified by LDH (KitMAK066, Sigma Aldrich, St. Louis, US). 400µl of 1% Triton-X100 (Sigma Aldrich, St. Louis, US) solution in PBS was used to lyse cells followed by three freezing and thawing steps.

Cell morphology was assessed by SEM (Zeiss 1530, Germany) at 6, 24, 48, and 72 h. Cells were fixed using a 2.5% glutaraldehyde solution in PBS at 4°C for 2 h, followed by 3 rinses in

PBS of 15 min each. Afterwards, a series of ethanol dehydration steps were carried out for 15 min each (10-30-50-70-90-99%). Finally, samples were vacuum dried and coated with Au/Pd to enhance conductivity. Image analyses of macrophage morphology were processed by FIJI (ImageJ software) to investigate the elongation ratio (N=30 except for β-TCP at 6h and TCPS at 72h, where N=10).

*Mesenchymal stem cell culture on heparinized substrates:* rMSCs were used to investigate the osteogenic potential of the heparinized surfaces. All samples were sterilized as previously described. Afterwards, 15x2mm$^2$ discs were left overnight in supplemented cell culture medium as preconditioning prior to seeding. rMSCs were cultured on the pristine and heparinized β-TCP discs ($8\cdot10^4$cells·ml$^{-1}$, 1ml) with Advanced DMEM (AdvDMEM) supplemented with 10% FBS, 2% HEPES and 1% of penicillin/streptomycin and L-glutamine (Invitrogen). TCPS was used as control. Cells were cultured over 6h, 3, 7 and 14 days refreshing medium every day. At day four, osteogenic medium consisting of supplemented advDMEM with 50 µg·ml$^{-1}$ ascorbic acid, 10 mM β- glycerophosphate and 100 nM dexamethasone was used as cell culture medium for all substrates. At each time point, samples were rinsed thrice with PBS and lysed with M-PER® (Mammalian Protein Extraction Reagent, Thermo Scientific, Waltham, MA, USA; 300 µl). Cytotoxicity Detection Kit LDH (Roche Applied Science, Penzberg, Germany) was used to quantify cell proliferation. The ALP activity was quantified as a marker of osteogenic differentiation (SensoLyte®pNPP Alkaline Phosphatase Assay Kit, AnaSpec). The results were expressed as a relative fold change compared to the cell number obtained on TCPS after 6 h and to the area of the discs.

*Osteoimmunomodulation of macrophage supernatants on rMSC:* The supernatants of the macrophage cell culture on the different substrates collected at 72h were used to study the osteoimmunomodulatory effects on rMSC, based on evaluation of the expression of osteogenic genes by RT-qPCR (**Table 1**). rMSC were seeded ($3\cdot10^4$cells·ml$^{-1}$, 0.3ml) using supplemented AdvDMEM on 48 well plates for 24h. After 24h, the media was replaced by

cytokine containing supernatants from the macrophage cell culture study at a 1:2 ratio. RNA was extracted at 1 and 3 days, and quantified with a spectrophotometer (NanoDrop ND-1000, Thermo Fisher Scientific Inc., USA). QuantiTect Reverse Transcription Kit (Qiagen GmbH, Hilden, Germany) was used for the synthesis of 100ng of complementary DNA. DNA templates were amplified using the primers shown in **Table 1** using QuantiTect SYBR Green RT-qPCR Kit (Qiagen GmbH, Hilden, Germany) in an RT-qPCR StepOnePlus (Applied Biosystems, Thermo Fisher Scientific Inc., Waltham, USA). RT-qPCR runs for specificity of primers was determined by melt curves analyses. Data was normalized by the expression of housekeeping gene (β-actin) and relative fold changes were calculated related to TCPS supernatant control at 1 day, according to the following equation:

$$E_{target}^{\Delta Cq\ target\ (TCPS\ 1d - sample)} / E_{housekeeping}^{\Delta Cq\ housekeeping\ (TCPS\ 1d - sample)}$$

where $C_q$ represents the median value of the quantification cycle of the triplicate of each sample and E corresponds to the efficiency of amplification, determined from the slope of the log-linear portion of the calibration curve, as $E=10^{(-1/slope)}$.

**Table 1.** Primers' sequences used for RT-qPCR (fw: forward; and rv: reverse).

| Gene | Gene symbol | Primer' sequences (5' to 3') |
|---|---|---|
| **β-actin** | ACTB | fw: CCCGCGAGTACAACCTTCT<br>rv: CGTCATCCATGGCGAACT |
| **Bone morphogenetic protein-2** | BMP-2 | fw: CCCCTATATGCTCGACCTGT<br>rv: AAAGTTCCTCGATGGCTTCTT |
| **Alkaline phosphatase** | ALP | fw: GCACAACATCAAGGACATCG<br>rv: TCAGTTCTGTTCTTGGGGTACAT |
| **Collagen** | COLL | fw: CATGTTCAGCTTTGTGGACCT<br>rv: GCAGCTGACTTCAGGGATGT |
| **Osteopontin** | OPN | fw: GTTTGAAGAAGGTGCAGAGGA<br>rv: GGTTCTGGCAGGGGTTTT |

*Statistical analysis:* Normality was checked through the Saphiro-Wilk test and normality plots for all experiments. ROS data are presented as mean±SD for n=6. Cytokine release, macrophage cell shape and gene expression data are presented as mean±SE, Cytokine release was performed using duplicates and three different donors (n=6), cell shape was calculated for

at least n=10 and gene expression was performed using triplicates of each material (n=3). One way ANOVA was used to assess statistical differences between groups, at an alpha value of 0.05, i.e. statistically significant difference was accepted for $p<0.05$. Levene's test was used to check for homogeneity of variance. Scheffe's post-hoc test was applied in case Levene's test was non-significant. In the case of significance, Tamhane's post-hoc was used. IBM SPSS Statistics was used for all statistical analysis.

**Acknowledgements**

The authors acknowledge the financial support provided by the Spanish Ministry, Project MAT2015-65601-R (co-funded by the EU through European Regional Development Funds), and by the Swedish foundation for international cooperation in research and higher education (STINT- IG2011-2047). MPG acknowledges the ICREA Academia award by the Generalitat de Catalunya. The authors thank Montserrat Domínguez for her technical support with XPS measurements, and BioIberica S.A. for providing the heparin used in this work.

Received: ((will be filled in by the editorial staff))
Revised: ((will be filled in by the editorial staff))
Published online: ((will be filled in by the editorial staff))

References

[1] H. Takayanagi, *Nat. Rev. Immunol.* **2007**, *7*, 292.

[2] J. R. Arron, Y. Choi, *Nature* **2000**, *408*, 535.

[3] M. Mittal, M. R. Siddiqui, K. Tran, S. P. Reddy, A. B. Malik, *Antioxid. Redox Signal.* **2014**, *20*, 1126.

[4] A. Mantovani, S. K. Biswas, M. R. Galdiero, A. Sica, M. Locati, *J. Pathol.* **2013**, *229*, 176.

[5] A. Mantovani, A. Sica, S. Sozzani, P. Allavena, A. Vecchi, M. Locati, *Trends Immunol.* **2004**, *25*, 677.

[6] D. M. Mosser, J. P. Edwards, *Nat. Rev. Immunol.* **2008**, *8*, 958.

[7] R. D. Stout, J. Suttles, *J. Leukoc. Biol.* **2004**, *76*, 509.

[8] Z. Chen, T. Klein, R. Z. Murray, R. Crawford, J. Chang, C. Wu, Y. Xiao, *Mater. Today* **2016**, *19*, 304.

[9] S. Chen, J. A. Jones, Y. Xu, H.-Y. Low, J. M. Anderson, K. W. Leong, *Biomaterials* **2010**, *31*, 3479.

[10] M. L. Godek, J. A. Sampson, N. L. Duchsherer, Q. McElwee, D. W. Grainger, *J. Biomater. Sci. Polym. Ed.* **2006**, *17*, 1141.

[11] P. C. S. Bota, A. M. B. Collie, P. Puolakkainen, R. B. Vernon, E. H. Sage, B. D. Ratner, P. S. Stayton, *J. Biomed. Mater. Res. Part A* **2010**, *95A*, 649.

[12] B. Wójciak-Stothard, A. Curtis, W. Monaghan, K. Macdonald, C. Wilkinson, *Exp. Cell Res.* **1996**, *223*, 426.

[13] Y. Arima, H. Iwata, *Biomaterials* **2007**, *28*, 3074.

[14] N. Faucheux, R. Schweiss, K. Lützow, C. Werner, T. Groth, *Biomaterials* **2004**, *25*, 2721.

[15] S. Pujari-Palmer, M. Pujari-Palmer, M. Karlsson Ott, *J. Biomed. Mater. Res. B. Appl. Biomater.* **2016**, *104*, 568.

[16] R. J. Schutte, A. Parisi-Amon, W. M. Reichert, *J. Biomed. Mater. Res. - Part A* **2009**, *88*, 128.

[17] Z. Chen, J. Yuen, R. Crawford, J. Chang, C. Wu, Y. Xiao, *Biomaterials* **2015**, *61*, 126.

[18] J. E. McBane, L. A. Matheson, S. Sharifpoor, J. P. Santerre, R. S. Labow, *Biomaterials* **2009**, *30*, 5497.

[19] V. Ballotta, A. Driessen-Mol, C. V. C. Bouten, F. P. T. Baaijens, *Biomaterials* **2014**, *35*, 4919.

[20] A. Mevoy, M. Jeyam, G. Ferrier, C. . Evans, J. . Andrew, *Bone* **2002**, *30*, 171.

[21] E. M. Sussman, M. C. Halpin, J. Muster, R. T. Moon, B. D. Ratner, *Ann. Biomed. Eng.*

**2014**, *42*, 1508.

[22] D. Bezuidenhout, N. Davies, P. Zilla, *ASAIO J. (American Soc. Artif. Intern. Organs)* **1992**, *48*, 465.

[23] T. Takada, T. Katagiri, M. Ifuku, N. Morimura, M. Kobayashi, K. Hasegawa, A. Ogamo, R. Kamijo, *J. Biol. Chem.* **2003**, *278*, 43229.

[24] S. Teixeira, L. Yang, P. J. Dijkstra, M. P. Ferraz, F. J. Monteiro, *J. Mater. Sci. Mater. Med.* **2010**, *21*, 2385.

[25] B. E. Uygun, S. E. Stojsih, H. W. T. Matthew, *Tissue Eng. Part A* **2009**, *15*, 3499.

[26] J. G. Cripps, F. A. Crespo, P. Romanovskis, A. F. Spatola, R. Fernández-Botrán, *Int. Immunopharmacol.* **2005**, *5*, 1622.

[27] K. R. Taylor, R. L. Gallo, *FASEB J.* **2006**, *20*, 9.

[28] L. Ramsden, C. C. Rider, *Eur. J. Immunol.* **1992**, *22*, 3027.

[29] M. S. Douglas, D. A. Rix, J. H. Dark, D. Talbot, J. A. Kirby, *Clin. Exp. Immunol.* **1997**, *107*, 578.

[30] S. J. Fritchley, J. A. Kirby, S. Ali, *Clin. Exp. Immunol.* **2000**, *120*, 247.

[31] G. M. Campo, A. Avenoso, S. Campo, A. D ’ascola, P. Traina, D. Samà, A. Calatroni, *J. Cell. Biochem* **2009**, *106*, 83.

[32] P. Dandona, T. Qutob, W. Hamouda, F. Bakri, A. Aljada, Y. Kumbkarni, W. . Shin, J. . Liao, G. . Gensini, G. . N. Serneri, *Thromb. Res.* **1999**, *96*, 437.

[33] G. Zhou, M. S. Niepel, S. Saretia, T. Groth, *J. Biomed. Mater. Res. Part A* **2015**, *104*, 493.

[34] J. Salbach, T. D. Rachner, M. Rauner, U. Hempel, U. Anderegg, S. Franz, J.-C. Simon, L. C. Hofbauer, *J. Mol. Med. (Berl).* **2012**, *90*, 625.

[35] V. Hintze, S. A. Samsonov, M. Anselmi, S. Moeller, J. Becher, M. Schnabelrauch, D. Scharnweber, M. T. Pisabarro, *Biomacromolecules* **2014**, *15*, 3083.

[36] V. Hintze, S. Moeller, M. Schnabelrauch, S. Bierbaum, M. Viola, H. Worch, D.

Scharnweber, *Biomacromolecules* **2009**, *10*, 3290.

[37] U. Hempel, C. Preissler, S. Vogel, S. Möller, V. Hintze, J. Becher, M. Schnabelrauch, M. Rauner, L. C. Hofbauer, P. Dieter, *Biomed Res. Int.* **2014**, *2014*, 938368.

[38] J. Salbach-Hirsch, S. A. Samsonov, V. Hintze, C. Hofbauer, A.-K. Picke, M. Rauner, J.-P. Gehrcke, S. Moeller, M. Schnabelrauch, D. Scharnweber, M. T. Pisabarro, L. C. Hofbauer, *Biomaterials* **2015**, *67*, 335.

[39] A. Irie, M. Takami, H. Kubo, N. Sekino-Suzuki, K. Kasahara, Y. Sanai, *Bone* **2007**, *41*, 165.

[40] J. Salbach, S. Kliemt, M. Rauner, T. D. Rachner, C. Goettsch, S. Kalkhof, M. von Bergen, S. Möller, M. Schnabelrauch, V. Hintze, D. Scharnweber, L. C. Hofbauer, *Biomaterials* **2012**, *33*, 8418.

[41] J. Salbach-Hirsch, J. Kraemer, M. Rauner, S. A. Samsonov, M. T. Pisabarro, S. Moeller, M. Schnabelrauch, D. Scharnweber, L. C. Hofbauer, V. Hintze, *Biomaterials* **2013**, *34*, 7653.

[42] M. Tichá, B. Železná, V. Jonáková, K. Filka, *J. Chromatogr. B Biomed. Sci. Appl.* **1994**, *656*, 423.

[43] U. König, A. Lode, P. B. Welzel, Y. Ueda, S. Knaack, A. Henß, A. Hauswald, M. Gelinsky, *J. Mater. Sci. Mater. Med.* **2014**, *25*, 607.

[44] S. Gittens, K. Bagnall, J. R. Matyas, R. Löbenberg, H. Uludag, *J. Control. Release* **2004**, *98*, 255.

[45] U. Edlund, S. Dånmark, A.-C. Albertsson, *Biomacromolecules* **2008**, *9*, 901.

[46] D. S. Bramono, S. Murali, B. Rai, L. Ling, W. T. Poh, Z. X. Lim, G. S. Stein, V. Nurcombe, A. J. van Wijnen, S. M. Cool, *Bone* **2012**, *50*, 954.

[47] Z. Chen, C. Wu, W. Gu, T. Klein, R. Crawford, Y. Xiao, *Biomaterials* **2014**, *35*, 1507.

[48] Z. Chen, A. Bachhuka, S. Han, F. Wei, S. Lu, R. M. Visalakshan, K. Vasilev, Y. Xiao, *ACS Nano* **2017**, *11*, 4494.

[49] W. Pompe, M. Gelinsky, A. Lode, A. Reinstorf, A. Bernhardt, U. Ko, *J Biomed Mater Res A* **2007**, *81*, 474.

[50] C. S. Goonasekera, K. S. Jack, G. Bhakta, B. Rai, E. Luong-Van, V. Nurcombe, S. M. Cool, J. J. Cooper-White, L. Grøndahl, *Biointerphases* **2015**, *10*, 04A308.

[51] A. Lode, A. Reinstorf, A. Bernhardt, C. Wolf-Brandstetter, U. König, M. Gelinsky, *J. Biomed. Mater. Res. A* **2008**, *86*, 749.

[52] F. Y. McWhorter, T. Wang, P. Nguyen, T. Chung, W. F. Liu, *Proc. Natl. Acad. Sci. U. S. A.* **2013**, *110*, 17253.

[53] G. A. Hudalla, J. T. Koepsel, W. L. Murphy, *Adv. Mater.* **2011**, *23*, 5415.

[54] M. S. Ahola, E. S. Säilynoja, M. H. Raitavuo, M. M. Vaahtio, J. I. Salonen, A. U. O. Yli-Urpo, *Biomaterials* **2001**, *22*, 2163.

[55] D. T. Hughes Wassell, G. Embery, *Biomaterials* **1997**, *18*, 1001.

[56] D. G. Belair, N. N. Le, W. L. Murphy, *Chem. Commun.* **2014**, *50*, 15651.

[57] R. Lever, A. Smailbegovic, C. Page, *Inflammopharmacology* **2001**, *9*, 165.

[58] R. Sridharan, A. R. Cameron, D. J. Kelly, C. J. Kearney, F. J. O'Brien, F. J. O'Brien, *Mater. Today* **2015**, *18*, 313.

[59] R. Klopfleisch, *Acta Biomater.* **2016**, *43*, 3.

[60] T. Lange, A. F. Schilling, F. Peters, F. Haag, M. M. Morlock, J. M. Rueger, M. Amling, *Biomaterials* **2009**, *30*, 5312.

[61] T. Lange, A. F. Schilling, F. Peters, J. Mujas, D. Wicklein, M. Amling, *Biomaterials* **2011**, *32*, 4067.

[62] R. Sridharan, A. R. Cameron, D. J. Kelly, C. J. Kearney, F. J. O'Brien, *Mater. Today* **2015**, *18*, 313.

[63] C. Dombrowski, S. J. Song, P. Chuan, X. Lim, E. Susanto, A. A. Sawyer, M. A. Woodruff, D. W. Hutmacher, V. Nurcombe, S. M. Cool, *Stem Cells Dev.* **2009**, *18*, 661.

[64] S. Mathews, S. A. Mathew, P. K. Gupta, R. Bhonde, S. Totey, *J. Tissue Eng. Regen.*

*Med.* **2014**, *8*, 143.

[65] M. Espanol, R. A. Perez, E. B. Montufar, C. Marichal, A. Sacco, M. P. Ginebra, *Acta Biomater.* **2009**, *5*, 2752.

[66] R. L. Williams, Development of Multifunctional Calcium Phosphate Particles for Drug Delivery and Formation of Cross-Linked Materials, University of Birmingham, **2014**.

[67] C. Dahlgren, A. Karlsson, *J. Immunol. Methods* **1999**, *232*, 3.

[68] G. Mestres, M. Espanol, W. Xia, C. Persson, M.-P. P. Ginebra, M. K. Ott, *PLoS One* **2015**, *10*, e0120381.

**Figure 1.** Physico chemical properties of the β-TCP discs. a) X-ray diffraction pattern; b) Pore entrance size distribution measured by MIP; c) SSA measured by nitrogen adsorption, and total open porosity according to MIP; and d) SEM image of the surface of the material.

**Figure 2.** Surface functionalization with heparin characterization. a) Effect of the immobilization method on the amount of heparin immobilized on the surface after 2h. The solution used had a heparin concentration of 100μg·ml$^{-1}$. Pristine samples, where heparin was adsorbed by physisorption, are compared to silanized samples, with two different silanization times, 1h or overnight (o.n.); data presented as mean±SD (n=3); b) Saturation of heparin onto the β-TCP surface. The silanized discs (overnight silanization) were immersed for 2h in solutions with different concentrations of heparin; data presented as mean±SD (n=3); c) XPS spectra of the pristine material (β-TCP), overnight silanized β-TCP (β-TCP-Sil) and heparinized β-TCP (β-TCP-H), this last prepared by 2h immersion of o.n. silanized samples in a 150μg ·ml$^{-1}$ heparin solution; d) SEM morphology of the surface of β-TCP-H, after heparin functionalization.

**Figure 3.** ROS release study on PMA-activated cells. Non-activated cells were used as negative control (TCPS). a) $H_2O_2$ release evolution profiles over time; b) Integration of the total area under the curves. Data presented as mean±SD, n=6, *p*-values calculated using one-way ANOVA and Scheffe's post-hoc test, $p < 0.05$. * indicates statistically significant differences compared to the negative control TCPS and # indicates statistically significant differences with respect to β-TCP.

**Figure 4.** Cytokine release by macrophages cultured on substrates for 6, 24, 48 and 72 hours. a) Tumor necrosis factor alpha (TNF-α); b) Interleukin 1 beta (IL-1β). TCPS+ and TCPS correspond to the positive and negative controls, with/without LPS stimulation respectively. * indicates statistical difference compared to positive control TCPS+, § to TCPS and # to β-TCP for each time point($p<0.05$). Data are presented as mean±SE of duplicate samples from three independent donors (n=6). *p*-values are calculated by one-way ANOVA with Tamhane's post-hoc test.

**Figure 5.** Representative SEM images of macrophages on β-TCP at 6h (a) and 72h (e); β-TCP-H at 6h (b) and 72h (f); TCPS at 6h (c) and 72h (g); TCPS+ corresponding to LPS stimulated cells at 6h (d) and 72h (h).Scale bar in images a, b, e, f: 10μm; c, d: 2μm; g, h: 20

µm, inset: 2µm. i) elongation ratio of cells at 6 and 72h. Data represented as mean±SE of a minimum of n=10, and *p*-values calculated by one-way ANOVA with Scheffe's post-hoc test. * denotes statistically significant differences from TCPS and TCPS+ at 72h, and # statistically significant differences between time points, $p<0.05$.

**Figure 6.** Cell proliferation and early differentiation of rMSCs cultured on β-TCP, β-TCP-H and TCPS as control. a) cell proliferation over time (14d) measured by LDH; b) Cell differentiation measured in terms of ALP activity over culture time. On day 4, the cell culture medium was replaced by osteogenic medium. * indicates statistically significant differences compared to control TCPS for the same time point ($p<0.05$) and # indicates statistically significant differences with respect to β-TCP for the same time point ($p<0.05$). Data presented as mean±SD (n=3) and *p*-values calculated by one-way ANOVA with Scheffe's post-hoc test.

**Figure 7.** Gene expression of rMSC at 1 and 3 days cultured in cytokine containing macrophage supernatants collected at 72h. Letters indicate statistical differences among substrates for each time point ($p<0.05$). Data are presented as mean±SE (n=3) and p-values calculated by one-way ANOVA with Tamhane's post-hoc test.

**Figure 8.** Diagram of the two heparin immobilization methods. a) physisorption and b) chemisorption.

**Table 2.** Primers' sequences used for RT-qPCR (fw: forward; and rv: reverse).

**Heparinized calcium phosphates represent an excellent platform to modulate osteoimmune response.** Heparinization offers a wide range of benefits observed by the down regulation of oxidative stress and inflammation, the improvement of MSC differentiation. Moreover, a coupling of inflammation and osteogenesis, investigated through the cytokine containing supernatants from macrophage cell cultures, is evidenced by a pro-osteogenic effect on rMSC.

**calcium phosphates heparinization**

*A. Diez-Escudero, M. Espanol, M. Bonany, X. Lu, C.Persson, M.-P. Ginebra**

**Heparinization of Beta Tricalcium Phosphate: Osteoinmunomodulatory Effects**

ToC figure